UILU-ENG 85-3606

Report No. 122

WEAR OF LASER PROCESSED CAST IRON

by

C. H. Chen,* M. K. Keshavan,**
C. J. Altstetter* and J. M. Rigsbee*

*Department of Metallurgy and Mining Engineering
University of Illinois, 1304 W. Green, Urbana, IL 61801

**Union Carbide Corporation
Engineering Products Division, P. O. Box 24184
Indianapolis, IN 46224

A Report of the

MATERIALS ENGINEERING - MECHANICAL BEHAVIOR

College of Engineering, University of Illinois at Urbana-Champaign

July 1985

TABLE OF CONTENTS

LIST OF TABLES

LIST OF FIGURES

WEAR OF LASER PROCESSED CAST IRON

C. H. Chen*, M. K. Keshavan**, C. J. Altstetter* and J. M. Rigsbee*

* Department of Metallurgy and Mining Engineering
University of Illinois, 1304 W. Green Street, Urbana, IL 61801;

** Union Carbide Corporation,
Engineering Products Division, P.O. Box 24184,
Indianapolis, IN 46224

Laser processing of ductile cast iron can produce surfaces with unique, metastable microstructures which are very erosion/abrasion resistant. This paper discusses relationships between the laser processing parameters, the resulting microstructures and the wear characteristics/mechanisms for slurry erosion and abrasion.

I. Introduction

The laser is a versatile surface processing tool since it allows precisely regulated amounts of energy to be delivered to a surface with precise spatial and temporal control. These characteristics allow surface processing to be done rapidly with minimal shape distortion and no need for an external quenchant. Laser surface treatments involving rapid heating of the surface and subsequent transformation hardening have found wide commercial acceptance [1]. The laser also allows treatment of hard-to-reach places and treatment in only those places where it is needed. Controlled surface hardening by a treatment such as laser processing will likely provide a cost-beneficial alternative in comparison to either bulk alloying or through-hardening heat treatment for wear resistance. General reviews of laser processing beyond the scope of this paper may be found in references 2 through 5.

Previous research into laser processing of cast iron can generally be classified into 3 categories: transformation hardening [6-8], hardening with surface melting [9-15] and rapid solidification with formation of an amorphous phase [16]. The laser transformation hardening process typically produces a martensitic matrix, containing flake or nodular graphite, with a measured hardness value of 600-700 HV [6-8]. Hardening with surface melting usually produces a mixed microstructure of retained austenite, cementite and martensite. Depending on the starting materials and processing parameters, the hardnesses vary considerably. As found in references 9 through 15, the hardnesses of the austenite range from 500-700 HV, while those of the cementite and austenite mixture range from 700-1200 HV. Snezhnoi et al. [16] demonstrated that localized areas of amorphous cast iron with a hardness up to 1200 HV can be obtained from a chilled cast iron by laser processing with a neodymium glass pulsed laser.

The objectives of this research are to improve the wear (erosion/abrasion) resistance of cast iron by laser hardening with surface melting and to correlate the enhanced wear resistance with the laser-induced microstructural changes. Ductile nodular iron specimens with a pearlite/ferrite matrix were examined, before and after laser treatment. The original and laser processed microstructures and hardnesses were correlated with the laser processing parameters and with the specimen erosion rates in SiO_2 in water slurries and abrasion rates in a rubber wheel/dry sand wear test.

II. Experimental Procedure

Ductile iron, graphite nodules in a pearlite/ferrite matrix, was chosen because of its common usage in industry. The ladle chemical analysis is shown in Table I. The alloy was sand cast from a 590 kg induction furnace heat as 5 cm x 10 cm x 60 cm bars. Specimens in the form of 2.22 cm x 3.18 cm x 0.25 cm coupons were machined from these bars and ground to finish of 0.5 μm.

Table I

Chemical Analysis

element	C	Si	S	P	Mn	Cr	Mo	Ni	Cu	Ti	Mg
wt. %	3.56	2.75	0.013	---	0.51	0.052	0.005	0.090	0.39	0.029	0.048

An AVCO EVERETT 10 kw CO_2 continuous wave laser, located in the Materials Engineering Research Laboratory, was used in this investigation. Its annular (TEM_{01}*) beam was focused by water cooled copper mirrors to a minimum diameter of approximately 1.0 mm, producing a power density of approximately 500 kW/cm^2 at a typical power level of 4 kW. Because metals are highly reflective [17] for 10.6 μm laser light, the surfaces of the samples were spray coated with a thin graphite layer to enhance absorption. They were then laser processed in a specially designed, controlled environment, laser processing chamber [18]. However, in this experiment, the cast iron samples were processed using helium shielding gas instead of a partial vacuum atmosphere. Unlike the previous

work [19], the laser beam energy was introduced directly into the chamber without the use of an infrared-transparent window and focused onto the sample surface. The samples were mounted on the periphery of a water cooled copper drum. The beam was stationary and the drum was rotated by a variable speed drive motor, giving the effect of beam scanning. In addition to this rotation, another drive motor axially translated the drum under the beam, allowing different surface areas to be processed. The overlapping of individual melt stripes was produced by the combination of high rotational speed with low translational speed. Helium gas was blown directly over the sample surface during laser processing to suppress plasma formation. The laser power levels used in this experiment ranged from 1 kW to 5 kW. The rotational speed, which ranged from 2 RPM to 30 RPM (corresponding to a tangential velocity of 1.67 cm/sec to 25.1 cm/sec) was coupled with the translational speed ranged from 0.06 cm/min to 0.8 cm/min, so that each point on the surface passed under the laser beam three times.

Erosion testing was carried out in a 20 ℓ enameled steel cylindrical tank with a cover. A slurry of roughly spherical SiO_2 particles in tap water was contained in the tank and was fluidized by rotating the samples in a manner such that they served as propeller blades, see [19]. The four sample holders were attached to a stainless steel shaft aligned along the axis of the tank. The samples were oriented face down, with their face normal at an angle of 45° relative both to the rotation axis and to their direction of travel. The shaft was rotated at a controlled speed of 575 ± 20 RPM (3 m/s, tangential velocity) with a variable torque-speed regulated motor. Four TEFLON baffles attached to the inside wall of the slurry tank ensured good mixing of the slurry by opposing the rotational and vortical motion induced by the rotating sample holder assembly.

Before testing, the samples were cleaned, weighed to an accuracy of ± 0.1 mg, and then coated with 0.15 mm thick thermosetting plastic to leave a 2 cm x 1.5 cm exposed area in the center.

A 50-70 mesh SiO_2 (average particle size 250 μm) was used to make a 35 wt.% (17 vol %) slurry. The testing was done in 4 hour increments, with both unprocessed and laser processed samples tested simultaneously to ensure uniformity of erosion conditions. After each test increment the protective coating was peeled off and the samples were cleaned and weighed. The samples were then recoated and the testing cycle was repeated, with total testing times up to 32 hours. Only a small (< 20°C) temperature rise was experienced during slurry testing.

Abrasive wear resistance of laser processed and unprocessed cast iron specimens was determined using the ASTM standard G65-80 low stress dry sand/rubber wheel abrasion test. Figure 1 is a schematic diagram of the test configuration. The samples were loaded against a chlorobutyl rubber wheel using 13.64 kg (30 lbs.) of force. Rounded quartz sand grains of size 50/70 mesh were passed between the sample and the 200 RPM rotating rubber wheel at a rate of 450 g/min. The weight loss after 1000 revolutions was measured and recorded for each sample. Calibration of the wear test was done using a standard-sized 1018 steel sample.

III. Results

A. Microstructure

The starting microstructure of the ductile cast iron, Figure 2, consisted of the usual pearlite matrix with graphite nodules surrounded by ferrite. These samples before laser processing had an average hardness of 228 HV.

More detailed microstructural characterization results for laser processed gray and ductile iron can be found in [19]. In this experiment, a

new series of laser processing conditions was examined. The microhardness and average melt depths are listed in Table II for each processing condition.

Table II. Hardness and melt depths as a function of processing

Power Level (kW) \ Rotational Speed (RPM)	2	3	5	8	12	20	25	30
1	—	0.21 / 763	0.14 / 713	0.08 / 529	0.04 / 556	—	—	—
2	0.42 / 977	0.36 / 1027	0.33 / 897	0.20 / 737	0.14 / 466	0.10 / 483	0.14 / 414	—
3	0.46 / 877	0.39 / 868	0.35 / 1014	0.28 / 830	0.22 / 633	0.17 / 513	0.30 / 515	0.13 / 478
4	—	—	—	—	0.28 / 763	0.23 / 536	—	0.17 / 454
5	—	—	—	—	0.65 / 986	0.35 / 648	—	0.26 / 545

Each cell: average melt depth (mm) / microhardness (HV)

1 RPM = a velocity of 0.83 cm/sec of the specimen relative to the laser beam

The melt depths and hardnesses measurements were made on polished and etched (2% nital) transverse cross-sections at the mid-width of each sample. The hardness values were determined with a microhardness tester using a load of 500 g on a square-based diamond pyramid. The indentation diagonal lengths ranged from 27 μm to 41 μm. The microhardness values are reported in units of HV (kg/mm^2). There were no significant hardness changes with respect to the melt depth. The reported microhardness values in Table II are the averages of 10 or more measurements taken on each specimen. The scatter in microhardness values between different locations within the laser processed zone of a single specimen was typically less than 10% of the average microhardness. Beyond the laser melt depth, hardness dropped rapidly to the original substrate value over the short distance of the heat affected zone.

Laser processing produced the three basic kinds of microstructures shown in Figures 3(a) to 3(c). Each figure is oriented so that the vertical direction indicates the specimen surface normal. For short laser/substrate interaction times and correspondingly high solidification rates the dendrite microstructures shown in Figure 3(a) is produced. This microstructure has an average hardness ranging from 400 HV to 650 HV. For long laser/substrate interaction times and low solidification rates the "feathery" ferrite and carbide composite microstructure shown in Figure 3(b) is produced. The typical microhardness of this microstructure ranges from 1000 HV to 1245 HV. Variation in the processing conditions to produce intermediate cooling rates produced mixtures of the feathery and dendritic microstructures and intermediate hardness levels. Generally, a network of cracks was observed with the feathery structure specimens. Fewer cracks were found in the mixed structure specimens and almost none were found in the dendritic microstructure.

The results of x-ray diffraction analyses (using Cu K_α radiation and a graphite monochromator) of the laser processed ductile irons are shown in Table III. The x-ray diffraction peak area ratio of $(111)_\gamma$ to $(110)_{\alpha,\alpha'}$ generally increased with decreasing laser/specimen interaction time. Figure 4 shows this effect for a series of specimens processed at 3 kW with a 10 fold variation in beam dwell time. This processing range produced a more than five fold change in austenite volume fraction.

B. Erosion

In this investigation, the slurry erosion resistance of one unprocessed and three differently laser processed ductile iron samples was tested. These latter three samples were processed so as to produce a wide variation in microstructure and hardnesses. As shown in Figure 5 and Table II, sample A

(2 kW, 8 RPM) has a hardness of 737 HV, sample B (2 kW, 25 RPM) has a hardness of 414 HV, sample C (2 kW, 3 RPM) has a hardness of 1027 HV. However it is evident in Figure 5 that after 32 hours of slurry erosion all three samples showed nearly identical erosion behaviors. With regard to the unprocessed material, the laser processing treatment improved erosion resistance by more than a factor of 3. Among the three processed samples the hardest, feathery structure of C produced the best erosion resistance, with the other two specimens being almost identical.

Table III. Microstructures and X-ray analyses

Power Level (kW) \ Rotational Speed (RPM)	2	3	5	8	12	20	25	30
1	—	M+D+F / 0.97	D+M / 1.11	D+α' / 1.48	D+α' / 1.56	—	—	—
2	F+M / 0.36	F / 0.63	M+F / 0.87	M+D+F / 1.20	D / 1.37	D / 2.50	D / 1.89	—
3	M / 0.25	M / 0.48	F / 0.84	M+D / 1.20	D+α' / 1.33	D / 1.48	D+α' / 1.27	D / 1.88
4	—	—	—	—	M+D / 1.20	D+M / 1.35	—	D / 1.83
5	—	—	—	—	M / 0.61	M+D / 0.87	—	D+M / 1.36

Micro-structure / X-ray area ratio $(111)_\gamma/(110)_{\alpha,\alpha'}$

F = Feathery microstructure

M = Mixture of feathery and dendritic microstructure

D = Dendritic microstructure

α' = martensite

Follwing erosion testing, the surfaces of eroded samples B (2 kW, 25 RPM) and C (2 kW, 3 RPM) were again examined by x-ray diffraction. Figure 6 compares the before-erosion and after-erosion x-ray diffraction scans of these two samples. Comparing the peak area ratios before and after erosion, there was little change noted for the feathery structure sample C (2 kW, 3 RPM). This was much changed, however, for the high austenite volume fraction,

dendritic matrix sample B (2 kW, 25 RPM). The surface microstructure for this sample clearly changed from an austenitic matrix before erosion to a predominately martensitic matrix with some retained austenite after erosion.

SEM micrographs, Figures 7(a) through 7(d), show the as-eroded surfaces of both the as-received and laser processed samples. The erosion time was 32 hours at 575 RPM (350 km total travel) for all specimens. For the as-received material, Figure 7(a) shows large erosion craters (~ 100 μm) and large wear debris (~ 10 μm). The erosion craters appear to be nucleated at the graphite nodules. Cracks are also visible in the regions surrounding the graphite nodule/matrix boundaries. Figure 7(b) of the dendritic microstructure (2 kW, 25 RPM) shows no obvious development of erosion craters. In some areas the dendritic microstructure is still visible while in other areas a featureless surface is present. At a higher magnification, Figure 7(c), some fine microcracks can be seen. The wear debris of this specimen is generally very small (≤ 1 μm). Figure 7(d) shows the as-eroded surface of the sample with a mixed structure (2 kW, 8 RPM). Again, the wear debris is small (≤ 1 μm), and appears to be generated mostly from the softer dendritic phase and along the cracks. The surface appearance after erosion of the feathery structure (2 kW, 3 RPM) resembles that of Figure 7(d). However, it has more of the stronger, feathery phase than the mixed microstructure.

C. Abrasion

Based on a total of one thousand revolutions with the ASTM standard low stress, dry sand rubber wheel abrasive wear test, the weight loss of each abraded specimen was plotted against its hardness value. Figure 8 shows that weight loss generally increased with decreasing hardness. After extrapolation to a hardness equivalent to that of the unprocessed material, it is observed that the abrasive wear of the unprocessed material is about 50% greater than

that after laser processing. It is notable that in spite of the large hardness range examined, the improvement in abrasive wear resistance with increasing hardness is small. The SEM micrographs in Figures 9(a) through 9(c) show the surface features of both the as-received and laser processed ductile cast iron samples after dry sand abrasion testing. Generally, the as-received sample had deeper and more numerous wear tracks and more wear debris. Wherever a graphite nodule is located, large wear debris particles (~ 15 μm), are observed. The 3 kW, 5 RPM laser processed sample had both the highest hardness (1014 HV) and the smallest (number per unit area) wear tracks and the least wear debris. The average size of the wear debris for this sample was around 2 μm. The 3 kW, 25 RPM laser processed sample had a hardness of 515 HV. The wear surface of this material was intermediate between that of the unprocessed and the highest hardness microstructure and the wear particles were around 2 μm in size.

Figure 10 shows the surface features of a feathery microstructure sample (3 kW, 5 RPM) around surface cracks both before and after abrasion testing. In Figure 10(a), before abrasion, the crack edge is smooth and featureless. In Figure 10(b), after abrasion, it is evident that severe deformation has occurred around the crack edge. It is observed that wear particles are being formed by a plastic deformation, smearing process. The arrows in 10(b) indicate two wear particles, in the upper portion of the crack, which have nearly separated from the surface.

IV. Discussion

A. Microstructure

Depending on the processing parameters of interaction time and power density, laser processing of ductile cast iron can produce three kinds of microstructures - dendritic (Figure 3(a)), feathery (Figure 3(b)) and mixed

(Figure 3(c)). The dendritic microstructure, which is obtained for short laser beam/specimen interaction times or low power densities, is comprised of austenitic dendrites and interdendritic carbides with usually very small amounts of ferrite and/or martensite. This microstructure has an average hardness ranging from 400 HV to 650 HV. The feathery structure, obtained at a long beam interaction times or high power densities, is comprised mostly of parallel carbides (cementite) and some ferrite, martensite and austenite. The typical microhardness of this structure ranges from about 1000 to over 1200 HV. At an intermediate beam interaction time or power density, a mixed structure with an intermediate hardness level can be obtained.

X-ray diffraction analyses, Table III and Figure 4, show that the amount of retained austenite increases with decreasing laser beam/specimen interaction time for a given power density. For a series of specimens processed at 3 kW with a ten fold variation in interaction time, a more than five fold change in austenite volume fraction is produced.

At a constant laser power density, rapid specimen translation relative to the fixed laser beam (i.e., a short interaction time) induces a high solidification rate. The austenitic dendrites retained by this processing have a very high carbon content (~ 1.8 wt. pct. C, see [19]), and thus are very stable, with an M_s far below room temperature. It has been found, however, that partial transformation to martensite can be induced by mechanical deformation at room temperature or quenching in liquid helium.

Laser processing with long interaction times or high power densities results in the feathery microstructure. According to an early study by Hume-Rothery [20], this is a plate-like eutectic microstructure which consists of parallel cementite plates separated by austenite which is not stable and may transform to martensite or pearlite. This plate-like eutectic can be formed

rapidly after marked supercooling and recalescence. The first phase to nucleate is a cementite plate which grows in a non-directional manner and causes the nucleation of new cementite plates parallel to the original plate. This microstructure is stronger than ledeburite and its formation always involves marked supercooling. This marked supercooling is favored by superheating the melt which reduces the number of available heterogeneous nucleation sites.

Sedunov et al. [13] reported results on similar cast iron with similar CO_2 laser processing conditions. They found that at a depth of ~ 1 μm the austenite and martensite comprise 20% each and cementite the remainder of the microstructure. With increasing thickness of the processed layer the quantity of cementite and austenite decreased while the amount of martensite increased. V. M. Andriyakhin et al. [14] found that the melted layer of their laser processed cast iron contained of a 3-phase mixture of austenite, cementite and ferrite. Tucker et al. [15] also found cementite, high carbon martensite (0.8 - 1.6 wt. pct. C) and retained austenite (0.4 - 1.9 wt. pct. C) to be present in the laser melted layer of near eutectic Fe-C binary alloys. The microstructure they obtained closely resembles the feathery microstructure in this investigation.

B. Erosion

The erosion test results (Figure 5) show that although the three laser processed samples have widely different microstructures and hardnesses they showed nearly identical erosion behaviors. With regard to the unprocessed material, the laser processing treatment improved erosion resistance by more than a factor of 3. A previous investigation on similarly processed cast iron [19] showed that slurry erosion improvement increases with increasing slurry erosion time.

Comparing the x-ray diffraction $(111)_\gamma$ and $(110)_{\alpha,\alpha'}$ peak area ratios before and after erosion, little change was noted for the feathery microstructure sample C (Figure 6). This was much changed, however, for the initially high austenite volume fraction dendritic matrix sample B. The surface microstructure for this sample clearly changed from an almost fully austenitic matrix before erosion to a predominantly martensitic matrix with some retained austenite after erosion. It is evident that the microdeformation processes ongoing during erosion are sufficient to induce an austenite to martensite transformation at the surface.

SEM examination of the as-received sample erosion surface, Figure 7(a), shows large erosion craters (~ 100 μm) and large wear debris (~ 10 μm). Cracks are also visible in the regions surrounding the graphite nodules. It appears that graphite nodules are vulnerable nucleation sites for erosion craters. After these soft nodules were eroded away, erosion occurred easily along the rims of these empty holes. Figure 7(b) shows an eroded surface for a dendritic microstructure sample. In some areas the dendritic microstructure is still visible while in other areas a smooth, featureless surface is present. This featureless surface apparently accounts for most of the austenite to martensite transformation, although a better understanding of this correlation needs further investigation. The fine microcracks present in this surface, Figure 7(c), likely come from the original dendrite/interdendritic carbide boundaries. The wear debris of this specimen is generally very small ($\leq$ 1 μm) and is roughly equal to or smaller than the average dendritic arm spacing. This indicates that the greatly refined laser processed microstructure causes a corresponding refinement in the wear particles eroded from the surface as well as a drastic increase in the energy required to erode away a given volume of surface. Figure 7(d) shows the as-eroded surface of a

sample with a mixed microstructure. Again, the wear debris is small ($\leq$ 1 μm) and appears to be generated mostly from the softer dendritic phase and along the cracks. The surface appearance after erosion of the feathery structure resembles that of Figure 7(d). However, it had more of the harder feathery phase than did the mixed microstructure. As a result, the feathery microstructure had a slightly better erosion resistance. On the other hand, although the dendritic microstructure sample had a relatively soft surface its erosion resistance was almost identical to the much harder mixed and feathery microstructures. It is suggested that martensite formation from the austenite dendrites may have been responsible for this.

C. Abrasion

Figure 8 shows that weight loss produced by the low stress, dry sand ASTM abrasive wear test generally decreases with increasing hardness. However, in spite of the large hardness range examined the improvement in abrasive wear resistance with increasing hardness is small. The SEM micrographs in Figures 9(a) through 9(c) show the surface features of both the as-received and laser processed ductile cast iron samples after abrasion testing. Generally because of the relatively soft matrix (230 HV) the as-received sample has deeper and more numerous wear tracks and more wear debris. Again, graphite nodules present vulnerable weak points for initiation of wear. Large wear debris ($\sim$ 15 μm) was observed surrounding graphite nodules. This observation may explain some of the difference in Figure 8 between the weight loss for the as-received material and the weight loss for an imaginary laser processed sample extrapolated to a hardness identical to that of the as-received material. The highest hardness (1014 HV) laser processed specimen (3 kW, 5 RPM) was observed to have the smallest (number per unit area) wear tracks and the least wear debris. The 3 kW, 25 RPM laser processed sample, with a hardness of 515 HV,

had a wear surface appearance intermediate between the unprocessed and feathery microstructures.

Another major factor for why the improvement in abrasive wear resistance with increasing hardness is small may be explained by the presence of surface cracks. Generally for these laser processed samples the higher the hardness the more numerous the cracks. Figure 10 shows clearly how the crack edge can be a preferred site for severe plastic deformation and wear particle generation.

V. Conclusion

Laser processing to induce rapid melting and resolidification of a thin surface layer on ductile cast iron can produce very erosion/abrasion resistant surfaces with a wide range of microstructures and hardnesses. Long beam/specimen interaction times and high power densities result in the development of a very hard (up to 1300 HV) feathery carbide/ferrite microstructure. Short beam/specimen interaction times and low power densities result in a softer (400 to 650 HV) dendritic microstructure composed of metastable austenitic dendrites with interdendritic cementite. The austenite is metastable with regard to mechanical deformation or cooling to liquid helium temperature. Intermediate beam/specimen interaction times and power densities produce a mixed structure with an intermediate hardness level. The tendency for surface cracking in the laser melted layer increases as the hardness increases.

Evaluation of the erosion properties of the laser processed surfaces was done by slurry erosion testing in aqueous SiO_2 slurry. The three laser processed samples tested having widely different microstructures and hardnesses, showed nearly identical erosion resistances. SEM micrographs show that although the dendritic microstructure is softer and weaker, the fact that

it has very few cracks helps its erosion resistance. SEM comparisons of the eroded surfaces also showed a dramatic decrease in wear particle size after laser processing. This change in wear particle size is thought to be the major cause of the improved erosion resistance and to result from both elimination of the graphite particles as potential erosion nucleation sites and from the increased hardness and greatly refined microstructures produced by laser processing. X-ray analyses before and after slurry erosion of the austenitic dendrite microstructure sample showed partial austenite to martensite transformation. It is also felt that this deformation-induced localized hardening of the surface during erosion can contribute to the improved wear resistance.

Evaluation of the abrasive wear characteristics of the laser processed cast irons was done by the standard ASTM low stress, dry sand/rubber wheel wear test. The abrasion resistance increased with increasing hardness but the improvement with increasing hardness is small. Explanation of this result is based partially on the fact that laser-induced surface cracks are prime wear particle nucleation sites and surface cracking increases with increasing laser processed layer hardness. Another important effect of laser processing is the near-elimination of the graphite nodules which are "weak points" in the microstructure around which wear particles can be easily generated. Finally, it is felt that retained austenite and its subsequent transformation to a very hard, high carbon martensite during the wear process plays an important role in enhancing the abrasive wear characteristics of the softer, dendritic microstructure.

Acknowledgements

The authors gratefully acknowledge the financial support of this research by the Materials Processing Consortium of the College of Engineering at the University of Illinois. This work was partially funded by the DOE Division of Materials Science under contract DOE-AC02-76ER01198. The work was also partially funded by the DOE Office for Coal Utilization under contract DOE-AC02-78ER10004. We would like to acknowledge use of the facilities in the Center for Microanalysis of Materials in the Materials Research Laboratory and the help of J. Culton and T. Casale in the operation of the laser in the Materials Engineering Research Laboratory. The cast iron was supplied courtesy of Caterpillar Tractor Company.

References

[1]. E. A. Metzbower, Ed., Source Book on Applications of the Laser in Metalworking, American Society for Metals, Metals Park, Ohio, 1981.

[2]. C. W. Draper, Journal of Metals, June, 1982, pp. 24-32.

[3]. E. A. Metzbower, Ed., Applications of Lasers in Materials Processing, American Society for Metals, Metals Park, Ohio, 1979.

[4]. K. Mukherjee and J. Mazumder, Eds., Lasers in Metallurgy, The Metallurgical Society of AIME, Warrendale, Pennsylvania, 1981.

[5]. M. Bass, Ed., Lasers Materials Processing, North-Holland Publishing Company, New York, 1983.

[6]. J. A. Wineman and J. E. Miller, Technical Paper IQ 77-372 Society of Manufacturing Engineers, Dearborn, Michigan, 1977.

[7]. D. Belfote, Lasers in Modern Industry, p. 128, J. F. Ready, Ed., Society of Manufacturing Engineers, Dearborn, Michigan, 1979.

[8]. P. J. Quick, General Motors Institute Technical Report, General Motors Corporation, Detroit, Michigan, August, 1978.

[9]. M. Yessik and R. P. Scherer, Lasers in Modern Industry, p. 139, J. F. Ready, Eds., Society of Manufacturing Engineers, Dearborn, Michigan, 1979.

[10]. V. E. Arkhipov, A. N. Grechin and M. L. Khina, Metal Science and Heat Treatment, 1980, Vol. 22, pp. 248-250.

[11]. V. M. Golubets, M. I. Moisa, Yu. I. Babei and G. V. Plyatsko, Soviet Materials Science, 1972, Vol. 8, pp. 505-506.

[12]. A. A. Zhukov, M. A. Krishtal, A. N. Kokora, Yu. I. Davydov and I. A. Goncharenko, Russian Castings Production, May, 1971, pp. 209-211.

[13]. V. K. Sedunov, V. M. Andriyakhin, N. T. Chekanova and V. M. Belov, Metal Science and Heat Treatment, 1980, Vol. 22, pp. 630-634.

[14]. V. M. Andriyakhin, N. V. Edneral, Kh. A. Mazorra, S. K. Orlov, Yu. A. Skakov and N. T. Chekanova, Izv. V.U.Z. Chernaya Metall., 1981, Vol. 24, No. 7, pp. 91-94.

[15]. T. R. Tucker, A. H. Clauer, C. T. Walters and S. L. Ream, Lasers in Metallurgy, p. 53, K. Mukherjee and J. Mazumder, Eds., The Metallurgical Society of AIME, Warrendale, Pennsylvania, 1981.

[16]. R. L. Snezhnoi, A. A. Zhukov and A. N. Kokora, Metals Science and Heat Treatment, 1980, Vol. 22, pp. 900-901.

[17]. Y. S. Touloukian and D. P. DeWitt, Eds., Thermophysical Properties of Matter, Vol. 7, p. 329, IFI/Plenum, New York, 1970.

[18]. M. L. Capp and J. M. Rigsbee, Journal of Materials Science and Engineering, 1983, Vol. 62, pp. 49-56.

[19]. C. H. Chen, C. J. Altstetter and J. M. Rigsbee, Metall. Trans. A, in press.

[20]. W. Hume-Rothery, The Structures of Alloys of Iron, 1st ed., p. 320. Pergamon Press Ltd., Oxford, 1966.

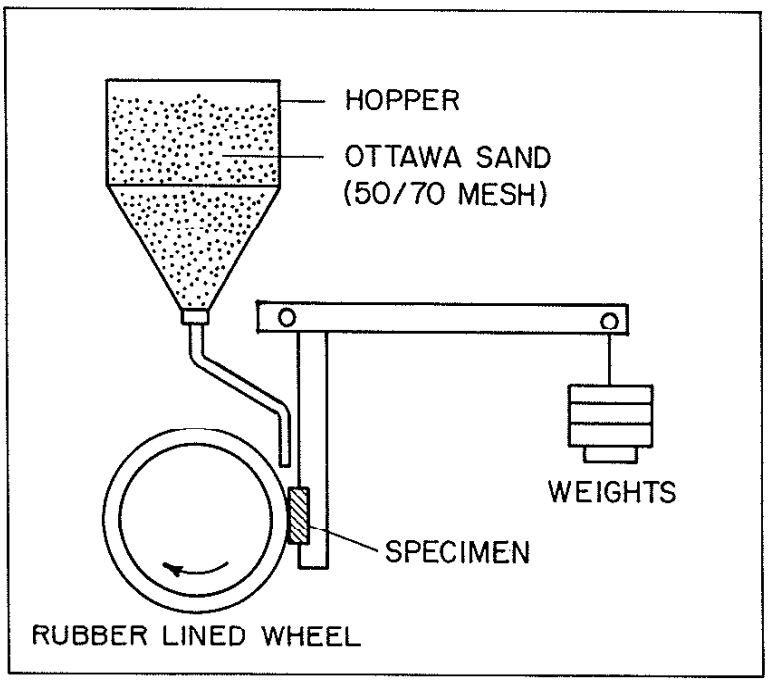

Figure 1. Schematic diagram of abrasive wear test configuration.

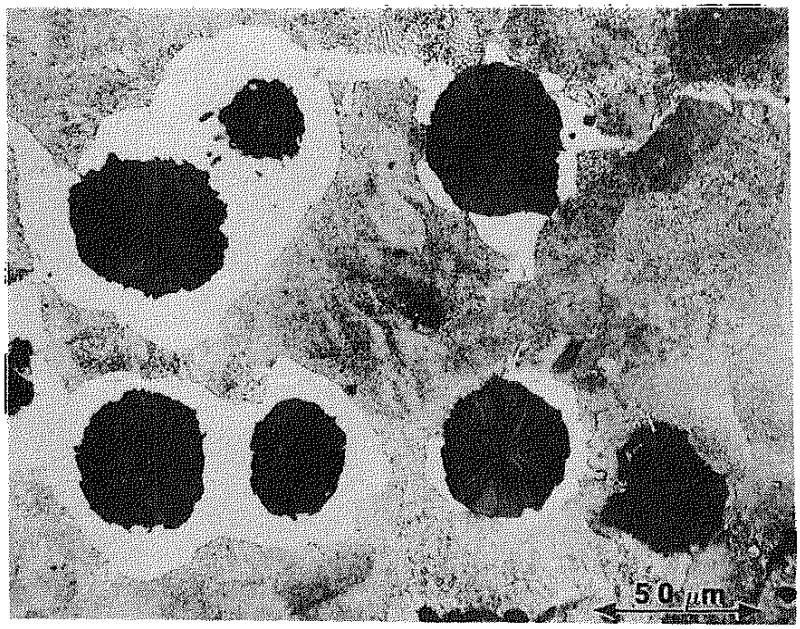

Figure 2. Microstructure of as-received ductile cast iron.

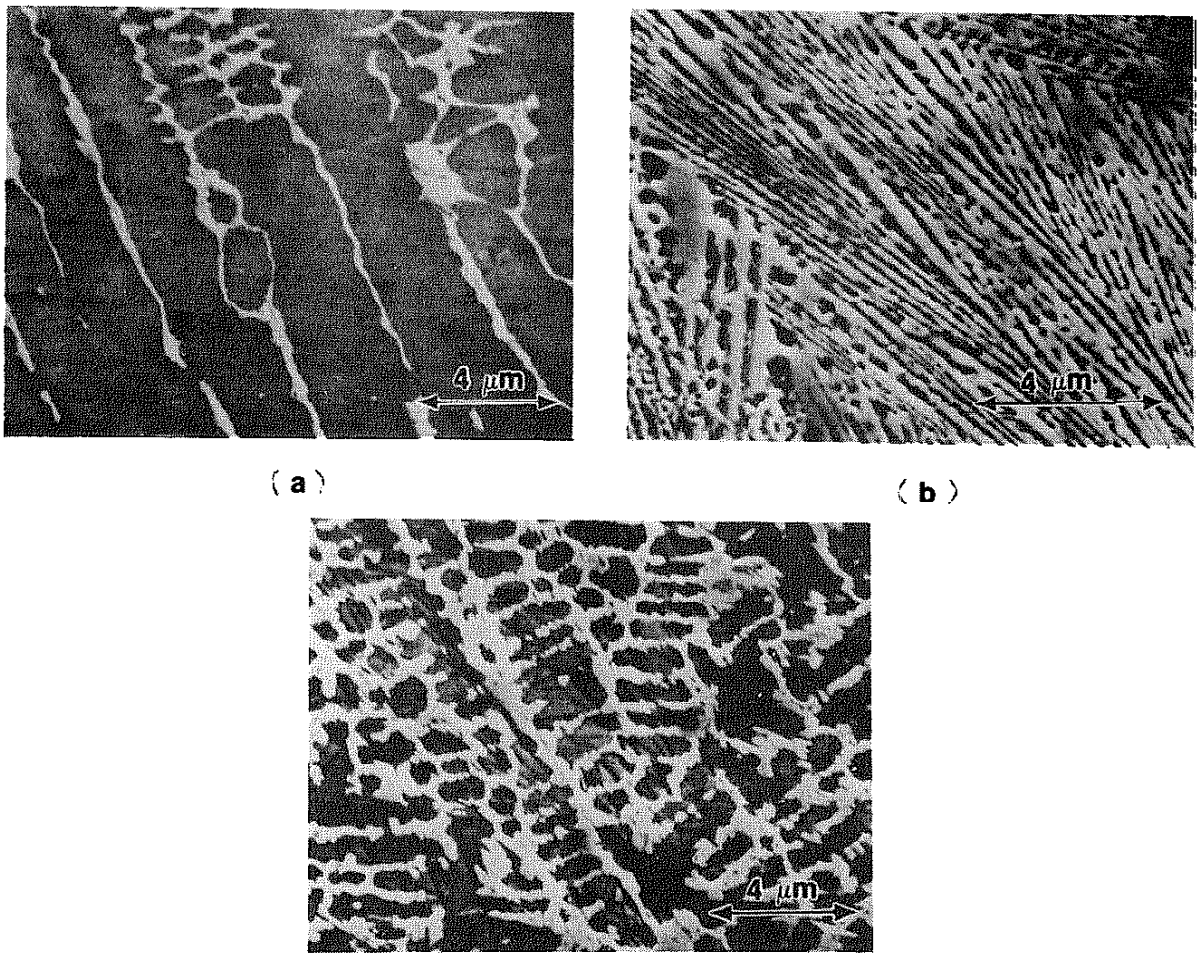

(a) (b)

(c)

Figure 3. SEM micrographs of laser processed microstructure

(a) dendritic structure 2 kW 12 RPM

(b) feathery structure 2 kW 3 RPM

(c) mixed structure 2 kW 8 RPM

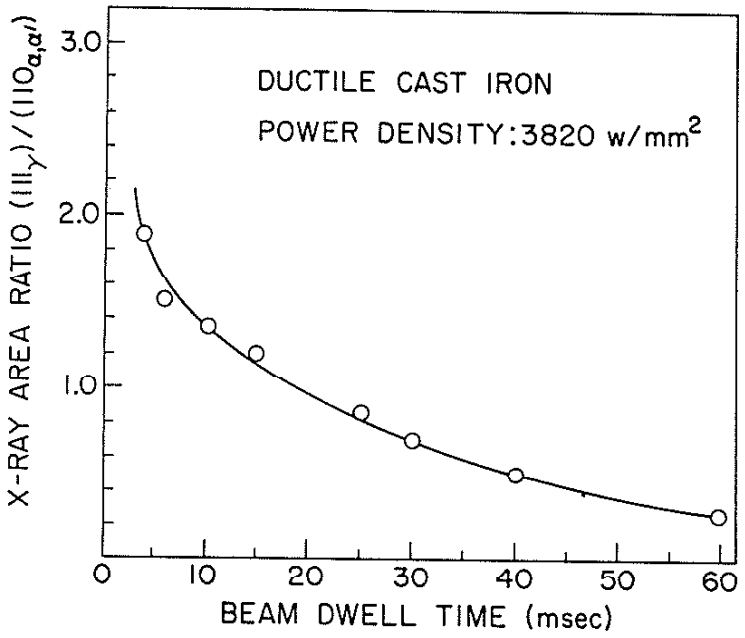

Figure 4. X-ray diffraction peak ratios of $(111)_{\gamma}$ to $(110)_{\alpha,\alpha'}$ as a function of beam dwell time.

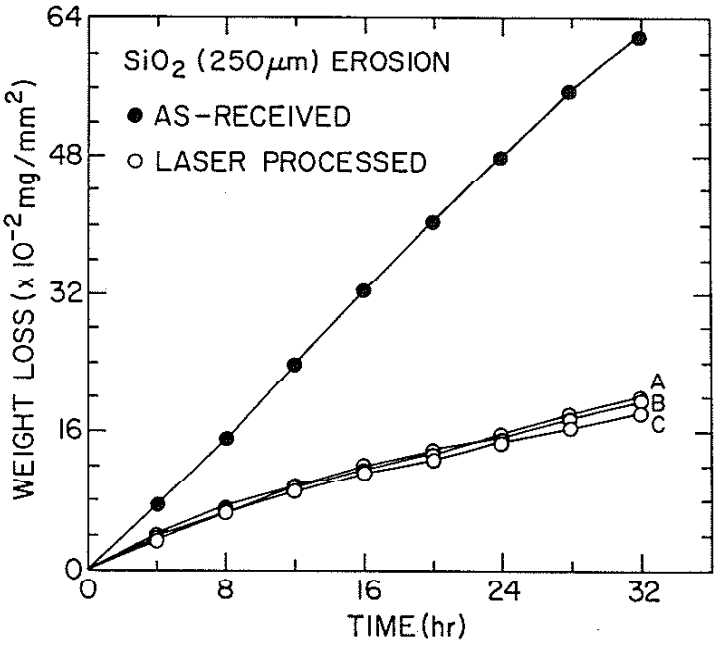

Figure 5. Erosive wear of as-received and laser processed samples (35 wt. pct. SiO_2 slurry, 32 h) (A = 2 kW, 8 RPM; B = 2 kW, 25 RPM; C = 2 kW, 3 RPM).

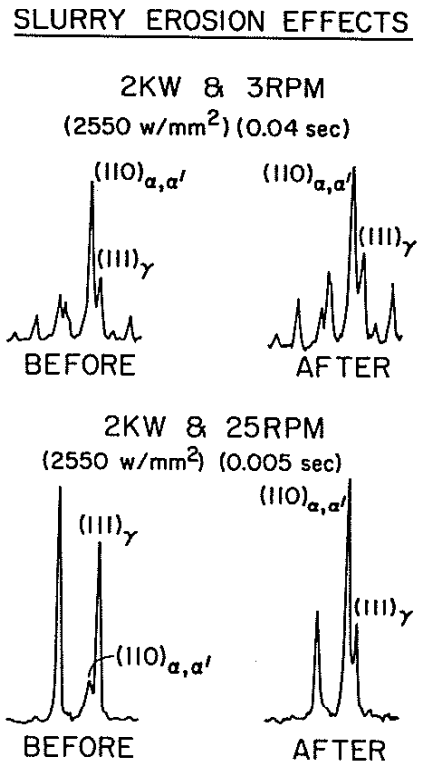

Figure 6. X-ray diffraction scans showing the effects of slurry erosion on the austenite microstructural constituent.

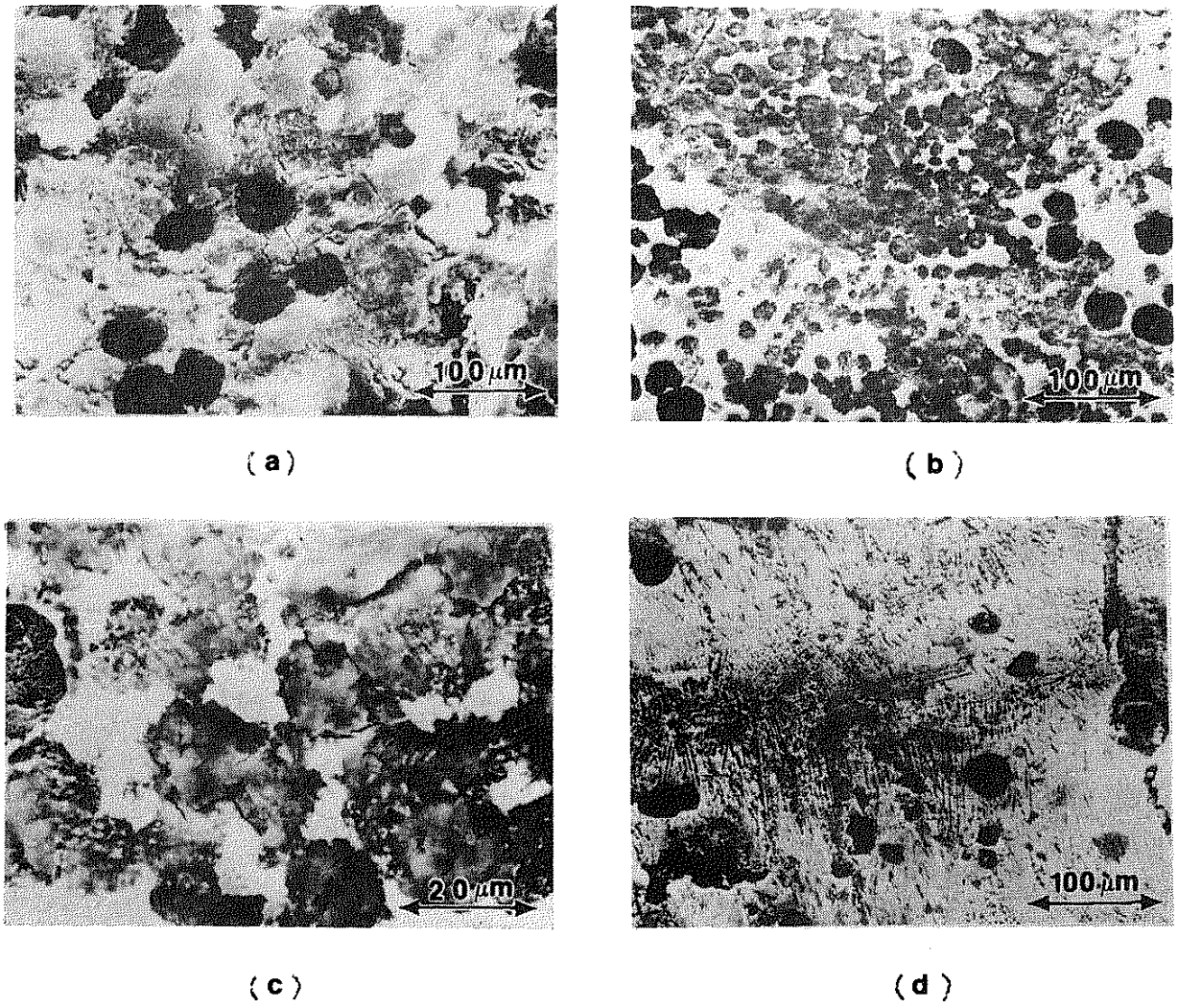

Figure 7. SEM micrographs of 32 hour slurry eroded ductile iron
(a) as-received; (b) laser processed (2 kW, 25 RPM);
(c) same as (b), higher magnification;
(d) laser processed (2 kW, 8 RPM).

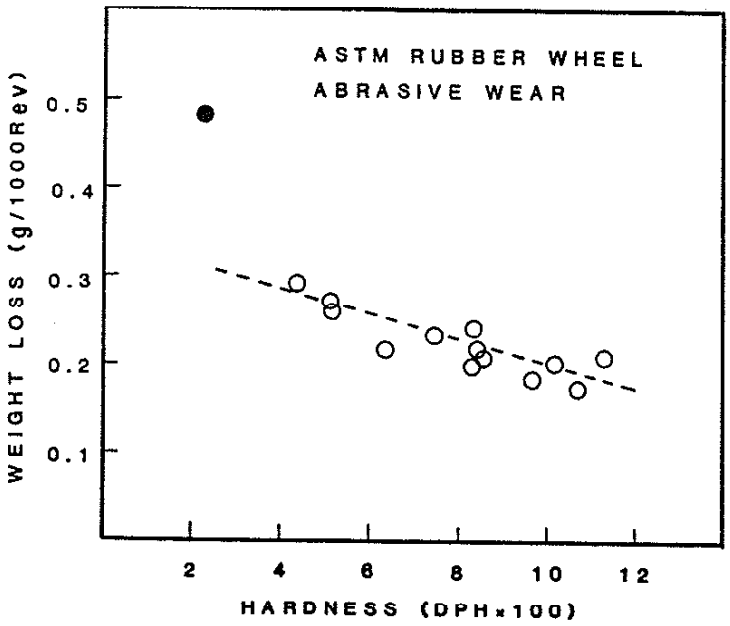

Figure 8. Weight loss by abrasion testing as a function of sample hardness

● unprocessed sample

○ laser processed sample

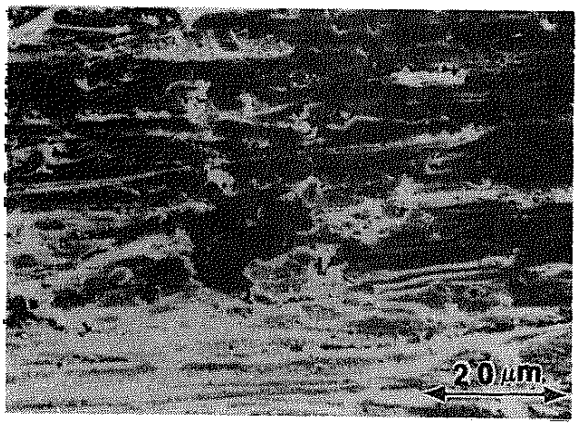

(a)

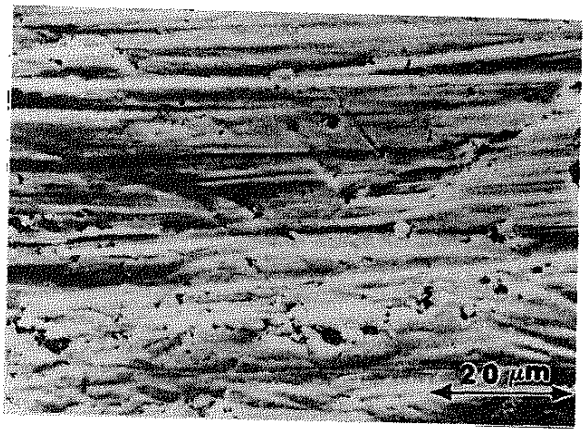

(b)

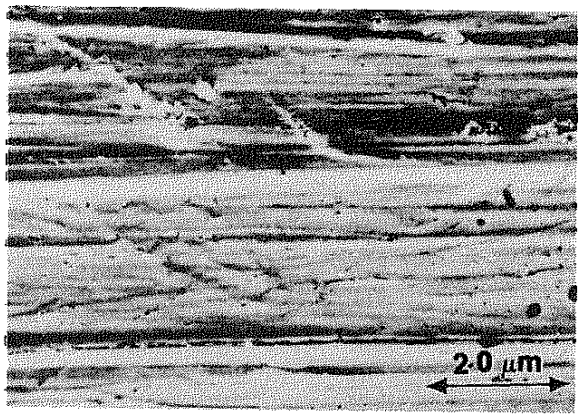

(c)

Figure 9. SEM micrographs of dry sand abraded ductile iron

(a) as-received

(b) laser processed (3 kW, 25 RPM)

(c) laser processed (3 kW, 5 RPM)

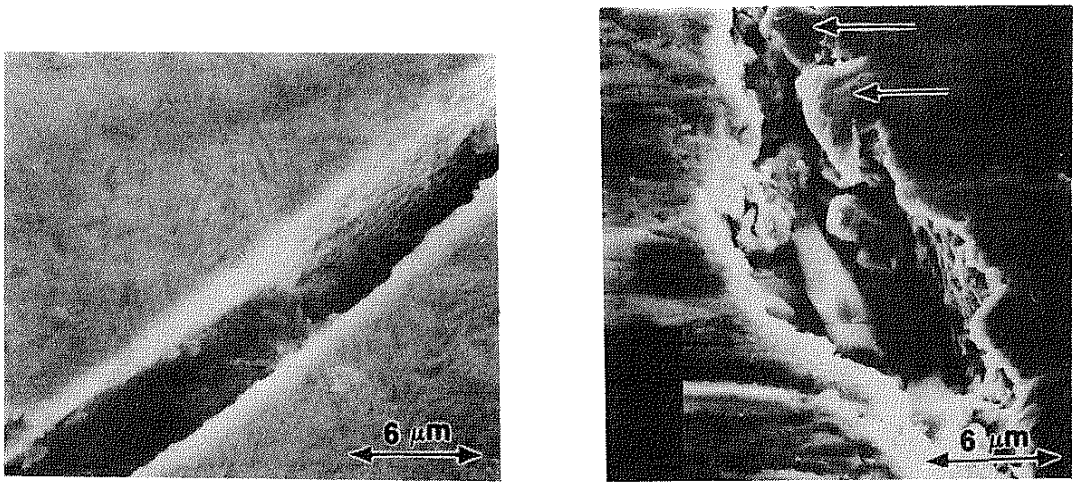

(a) (b)

Figure 10. Surface feature around a surface crack in laser processed (3 kW, 5 RPM) ductile iron.

(a) before abrasion

(b) after abrasion